Fabrication of large binary colloidal crystals with a NaCl structure

E. C. M. Vermolen, A. Kuijk, L. C. Filion, M. Hermes, J. H. J. Thijssen[1], M. Dijkstra, and A. van Blaaderen[2]

Soft Condensed Matter, Debye Institute for NanoMaterials Science, Utrecht University, Princetonplein 1, NL-3584 CC Utrecht, The Netherlands

Binary colloidal crystals offer great potential for tuning material properties for applications in, for example, photonics, semiconductors and spintronics, because they allow the positioning of particles with quite different characteristics on one lattice. For micrometer-sized colloids, it is believed that gravity and slow crystallization rates hinder the formation of high-quality binary crystals. Here, we present methods for growing binary colloidal crystals with a NaCl structure from relatively heavy, hard-sphere-like, micrometer-sized silica particles by exploring the following external fields: electric, gravitational, and dielectrophoretic fields and a structured surface (colloidal epitaxy). Our simulations show that the free-energy difference between the NaCl and NiAs structures, which differ in their stacking of the hexagonal planes of the larger spheres, is very small ($\approx 0.002\ k_{\mathrm{B}}T$). However, we demonstrate that the fcc stacking of the large spheres, which is crucial for obtaining the pure NaCl structure, can be favored by using a combination of the above-mentioned external fields. In this way, we have successfully fabricated large, 3D, oriented single crystals having a NaCl structure without stacking disorder.

colloidal materials | photonic crystals | self-assembly | surface patternings (epitaxy)

Fig. 1. NaCl unit cell and a confocal image of a hexagonal layer in a NaCl colloidal crystal grown by sedimentation. (*A*) Schematic representation of the conventional unit cell of the NaCl structure, where the green spheres represent the large colloids and the red spheres represent the small colloids, both in their own fcc structure. (*B*) Confocal scanning *xy* image of a NaCl crystal grown by sedimentation. Only the fluorescent cores of the particles are visible in the confocal images. (Scale bar: 10 μm.)

Recently, examples have been shown of the tunability of binary colloidal crystals in several binary systems of nanoparticles (1–5). This tunability of the material properties offers great potential for applications in materials science. However, in many cases, the absolute size of the building blocks is of crucial importance for the functionality of the material. For example, to obtain a photonic band gap in the visible or near-infrared range, which is important for applications in telecommunications, the lattice spacings have to be of the order of 0.1 to 1 μm. Unfortunately, for larger colloids, gravity and slow crystallization rates hinder the formation of binary crystals (6–8). We recently found in calculations that a so-called inverse photonic crystal based on the binary sodium chloride has a larger band gap than that of an inverse fcc crystal which until now has been the structure almost exclusively focused on in methods using self-assembly (see *SI 1* in the *SI Text* and Fig. S1). The finding of this property of the NaCl binary lattice motivated us to focus on this binary crystal, but the methods we present for the manipulation of the growth of high-quality binary crystals from dispersions of micrometer-sized spheres are quite general (see also *SI 2* in the *SI Text* and Fig. S2). For instance, the results presented in this paper also directly indicate how to grow other binary crystals as discussed in the conclusion section. We explore here several combinations of external fields to optimize the number of small particles in the NaCl structure and to avoid stacking faults. The binary NaCl crystal structure consists of spheres of two different radii (σ_{L} and σ_{S}), both ordered in a fcc structure, where the small particles are in the octahedral holes of the fcc crystal of the large spheres (Fig. 1*A*). For a close-packed fcc crystal of the large spheres, the radii of the small spheres (σ_{S}) have to be smaller than $0.41\ \sigma_{\mathrm{L}}$ for them to fit in the octahedral holes but larger than $0.22\ \sigma_{\mathrm{L}}$, the radius of the tetrahedral holes in the fcc crystal. The stability of the NaCl structure in binary hard-sphere dispersions has been studied both theoretically (9, 10) and by simulations
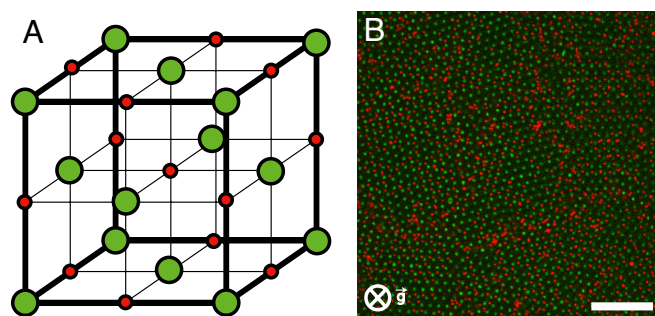
(11–13). From these studies, it can be concluded that NaCl is stable in the approximate size–ratio range $0.2 < \sigma_{\mathrm{S}}/\sigma_{\mathrm{L}} < 0.45$ (10, 11). NaCl structures have been observed in nanosphere systems (2, 14) and oppositely charged colloidal systems (15). In addition, a colloidal NaCl structure has been fabricated by layer-by-layer growth (16), but this method is time-consuming and is not suitable for more than a few layers. Hard-sphere NaCl crystals have been grown following homogeneous nucleation from a binary dispersion (17, 18), but the stacking order of the larger spheres could not be determined or was only determined very locally.

Similarly as for single-component hard-sphere crystals, the stacking sequence of the close-packed planes of the large spheres can be *ABA* instead of *ABC*, which gives an hcp structure instead of an fcc structure. In that case, if the octahedral holes are filled up with small spheres, the corresponding binary crystal structure is that of NiAs. As the free-energy difference between fcc and hcp crystals is very small (19), one might expect that the free energies of NaCl and NiAs are very similar as well. We studied the stability of NaCl and NiAs by using the Frenkel and Ladd method (39) and found that NaCl is thermodynamically the most stable structure, although with a free-energy difference of only $\approx 0.002\ k_{\mathrm{B}}T$ per particle for a size ratio of $\sigma_{\mathrm{S}}/\sigma_{\mathrm{L}} = 0.3$. Because the free energies of these two structures are nearly equal, one expects a random stacking sequence of the large spheres as is
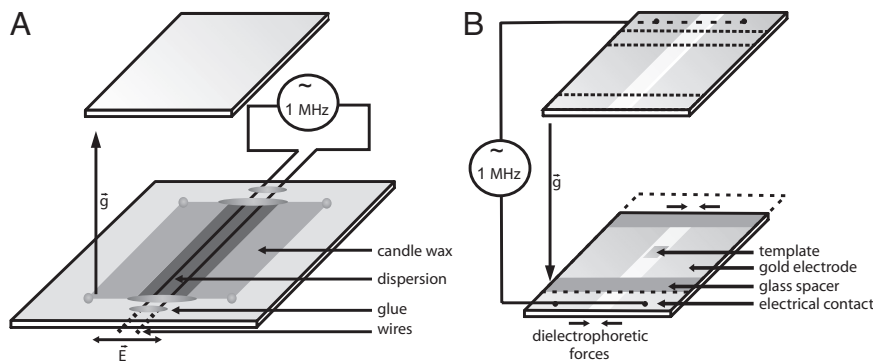
APPLIED PHYSICAL SCIENCES

Fig. 2. Sample cell designs. (*A*) Sample cell used for crystal growth by sedimentation, directed by an electric field. (*B*) Sample cell used for crystal growth by compressing with dielectrophoretic forces, directed by a templated bottom wall.

found for single-component hard-sphere systems (20). Despite this tiny free-energy difference, we demonstrate here that the NaCl structure, rather than the NiAs structure, can be favored in the growth of binary colloidal crystals by employing a combination of external fields.

The rest of the paper is organized as follows. We start by describing the experiments with gravity-induced crystallization from a binary mixture of micrometer-sized silica spheres. Subsequently, we describe the effects on binary-crystal growth of external electric fields and we consider binary crystals fabricated by using colloidal epitaxy. Finally, we combine colloidal epitaxy with dielectrophoretic compression, demonstrating the potential of combining external fields to improve the quality of binary colloidal crystals. All of these fields were previously explored by our group for one-component systems (20–27), but they have never before been applied to binary systems.

Gravity-Induced Crystallization. Experimentally, we first studied a binary mixture of silica spheres in DMSO under compression by gravity. With $\sigma_L = 1.37$ μm and $\sigma_S = 0.41$ μm, the silica spheres had a size ratio of $\sigma_S/\sigma_L = 0.3$. To allow imaging into separate channels in confocal laser scanning microscopy, the cores of the large spheres were labeled with FITC, whereas those of the small spheres were labeled with RITC (for synthesis details, see *Synthesis*). The refractive-index matching solvent caused a steep, almost hard-sphere-like interaction potential, resulting from charges on the surface and background ions in the dispersion (20). These first experiments resulted in binary structures with small crystal domains (of the order of 20 μm × 20 μm) in which hexagonal (111) planes of large spheres were parallel to the bottom wall for most of the domains (Fig. 1*B*). This orientation is favored by sedimentation on a flat bottom wall (20).

We determined the stacking parameter of the structures as described in *Image Analysis*. For the sedimented binary structures, a stacking parameter α of approximately 0.7 was found, indicating that the structure had a fair amount of randomness in its stacking sequence of (111) planes but with a preference for fcc stacking. In other words, the binary crystals which were formed did not have a pure NaCl structure but consisted instead of a mixture of NaCl and NiAs. These stacking errors, as well as the small domain size, can be disadvantageous for their use in technological applications.

Electric-Field-Assisted Crystallization. To increase the domain size of the crystals and obtain additional control over the orientation of the crystals, we succeeded in directing the crystallization of the sedimenting binary mixture by a horizontal external electric field, perpendicular to gravity (Fig. 2*A*). A one-megahertz oscillating electric field of 200 V peak to peak was used between wires which were 1.3 mm apart. The one-megahertz AC field

ensured that the double layer around the colloids did not polarize (24, 28), whereas the relatively low electric-field amplitude made sure that only the large colloids obtained a significant dipole moment $\vec{p}$, as this is proportional to the particle volume. In earlier work, it has been shown that for single-component dispersions at high field strengths, the dipolar interactions favor a body-centered tetragonal colloidal crystal lattice (22, 24, 29). However, for low fields, where the gravitational and dipolar energy start to compete (24, 25), one finds oriented fcc crystals (22, 24). It was also found that frequently turning the sample upside down caused a complicated sedimentation behavior (24, 30, 31), which resulted in annealing of the crystals. Similar observations were made in our binary system. We observed crystals oriented with the hexagonal planes parallel to the substrate near the bottom of the cell (Fig. 3), such that strings of nearly touching particles in these planes were along the field direction, in addition to a higher stacking probability of fcc than hcp ($\alpha \simeq 0.7$). Moreover, turning the sample upside down resulted in larger single crystal domains with a size of roughly 30 μm × 30 μm.

By using confocal microscopy, we observed the crystallization process in time, which already started in the bulk as homogeneous crystallization after 10 min because of the induced dipole moments of the large colloids. Heterogeneous crystallization from the bottom wall upward took over when the dispersion was compressed further by gravity. This combination of homogeneous and heterogeneous crystallization [which was not observed in the single-component case (24)], resulted in crystals with the (111) plane parallel to the lower glass wall near the bottom of the sample and a varying orientation of the crystals higher up in the sample. However, as before, the close-packed strings aligned in the direction of the electric field (Fig. 3*A*). As was observed in the crystals presented in refs. 24 and 32, it was found that the interparticle distance in the direction of the electric field was slightly smaller than in the other directions. However, this distortion, caused by the softness in the interparticle potential in combination with the anisotropy of the dipolar interactions, was small (the ratio between the particle distances in the different directions was 0.97).

Because of the different sedimentation rates of the two sizes of colloids, there were many small particles on top of the crystals and fewer than the stoichiometric amount at the bottom. Consequently, not all octahedral holes were filled with small particles, and the ratio of the number of small particles to the number of large particles in the crystal, f_N^{crystal}, was not equal to 1, as it should be for NaCl. We determined the relative number ratio in the crystal from confocal microscopy data as described in *Image Analysis*. By changing the initial number ratio between large and small particles in the dispersion, we could increase the parameter f_N^{crystal} in the crystals directed by the electric field from 40% for
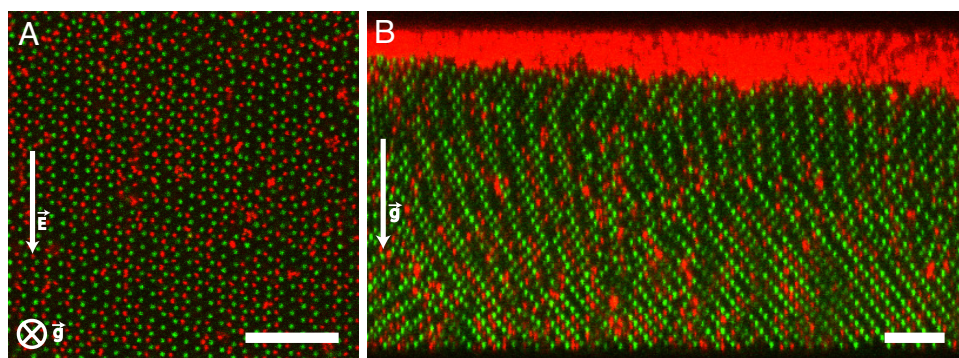
Fig. 3. Confocal scanning images of a NaCl colloidal crystal grown in an external electric field. (*A*) *xy* scan of the (111)-plane. (*B*) *xz* scan of crystals with their (111)-plane horizontal. Only the fluorescent cores of the particles are visible in the confocal images. (Scale bars: 10 μm.)

an initial number ratio of $N_S/N_L = 1$ to 89% for $N_S/N_L = 10$. However, the number of vacancies in the crystal of the large particles also increased from 1.5% to 5%. From confocal images, it was apparent that the assembly of small particles on lattice sites of large particles was causing the formation of more point defects.

Epitaxial Growth. Controlling the orientation of colloidal crystals can also be done in another way—by sedimentation on a structured wall (21, 23), referred to as colloidal epitaxy. This method yielded binary crystal domains that were as large as the template, which in our case was a 2D hole array made by soft lithography, extending over several hundreds of micrometers in both dimensions. By choosing an appropriate template, the desired crystal structure could be selected. In our case, the (100) fcc face (a square structure with a spacing of 1.42 μm, only slightly larger than the close packing distance between the larger particles) directed the growth of the large particles such that only an fcc structure formed, yielding one single binary crystal. The NiAs (hcp-stacked) structure cannot grow on this template because a square face does not exist in the hcp structure. Instead of DMSO, the solvent in the dispersions for these sedimentation experiments was a mixture of glycerol and water that matched the index of refraction of the silica spheres. The lattice parameters of the resulting crystals were not distorted in any direction, i.e., the spacing in the (100) plane stayed 1.42 μm in both horizontal directions up to at least the fifth layer. The highest f_N^{crystal} we obtained by using sedimentation on a square template was 60% for $N_S/N_L = 10$.

Dielectrophoretic Compression on an Epitaxial Template. To increase f_N^{crystal} in epitaxial growth, we used a technique recently introduced as the "electric bottle" (27, 33). We compressed the binary dispersion horizontally by dielectrophoretic forces created by electric-field gradients, thereby leaving less time for the binary dispersion to separate under gravity. The compression cell was formed by two horizontal plate electrodes with a slit in both electrodes. The cell design is shown in Fig. 2*B*. When a one-megahertz oscillating electric field of $\approx$30 V (peak–peak) is applied between the electrodes, which are $\approx$140 μm apart, there are significant field gradients at the edges of the slit. These field gradients apply a pressure to the enclosed dispersion and forces the colloids, which have a dielectric constant that is lower than that of the liquid, into the field-free region in the slit. We used the same glycerol/water solvent mixture as in the sedimentation experiments on a template, which was on the bottom of the slit. In this way, f_N^{crystal} could be increased to 73%, yielding a large, template-sized NaCl single crystal without lattice distortions. The (100)-oriented NaCl crystal in the slit was 25 layers thick. Confocal images of the crystal in the slit are shown in Fig. 4.

The spacing of the hole array, used for the epitaxial growth of the NaCl binary colloidal crystals, was chosen as close as possible to the effective radius of the large spheres in the dispersion. However, as was shown by Hoogenboom (34), the growth of a crystal is very sensitive to the spacing of the epitaxial template. A mismatch of a few percent leads to stress in the crystal. A mismatch of a template and a crystal can even completely prevent a crystal with the intended crystal face from nucleating at the template (21, 26).

The stress in the NaCl crystals expressed itself in defects that were primarily visible in the (100) planes. The stress in the crystals was probably due to the mismatch of the template and the ideal crystal or due to interstitials. Confocal microscopy images of the (100) planes show clear defect lines under 45° with the horizontal, above or below which the (100) plane is not in focus of the microscope (see for example Fig. 5*A*). Parts of the
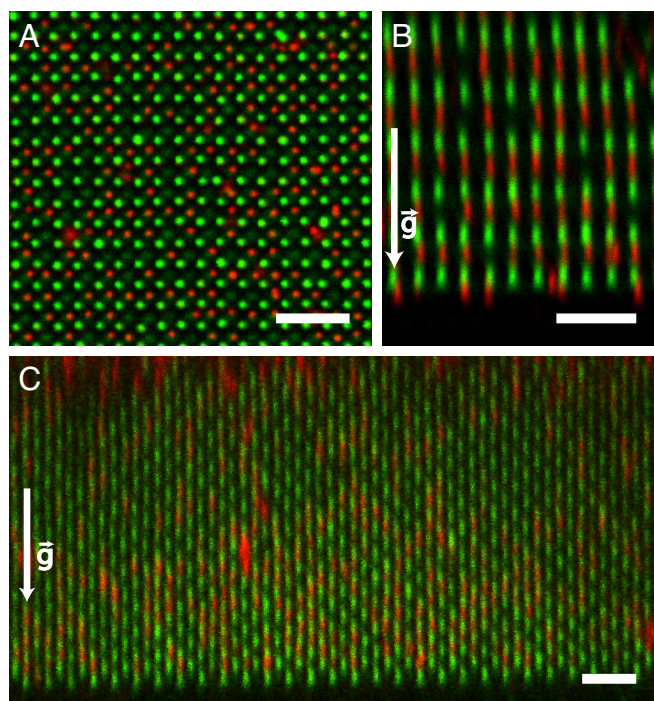

Fig. 4. Confocal scanning images of a NaCl colloidal crystal grown on a template by compression with dielectrophoretic forces. (*A*) *xy* scan of the (100)-plane. (*B*) *xz* scan of the (110)-plane. (*C*) *xz* scan of the (100)-plane. Only the fluorescent cores of the particles are visible in the confocal images. Note that not all small spheres are visible, because they are more easily out of focus. (Scale bars: 5 μm.)
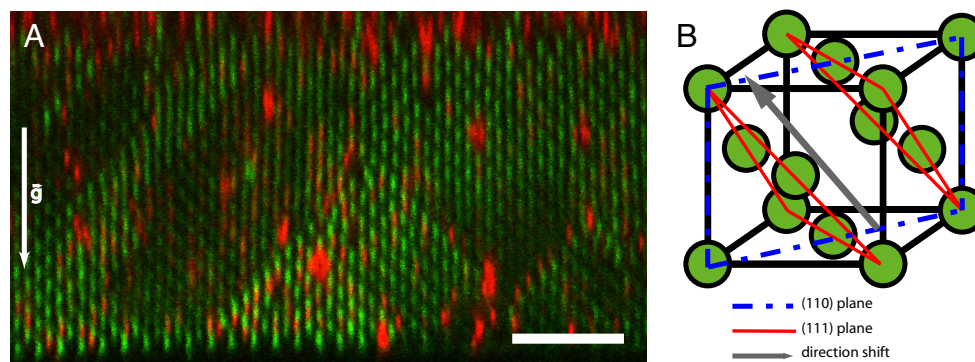
Fig. 5. Stress-induced stacking defects in epitaxially grown NaCl colloidal crystals. (*A*) Confocal *xz* scan of the (100)-plane of a NaCl crystal grown on a template by compression with dielectrophoretic forces. Only the fluorescent cores of the particles are visible in the confocal microscopy images. Note that not all smaller spheres are visible because they are often out of focus. (Scale bar: 10 μm.) (*B*) Schematic image illustrating the direction of the shift of the crystal domains. For clarity, only the large spheres are depicted, which form an fcc lattice. The dash-dot-dash lines indicate the (110) plane and the dashed lines indicate the (111) plane. To release stress, the crystal domain slides over the (111) plane in the direction of the intersection between the (110) plane and the (111) plane. This direction is indicated with the gray arrow.

crystal are shifted along the (111) planes, bringing them out-of-plane along the (100) plane. The same defects were found in single-component fcc crystals grown by dielectrophoretic compression on a square template (35).

The shift of the planes is illustrated in Fig. 5*B*: The two fcc crystals are shifted along the (111) planes in a direction that is parallel to the intersection line of the (110) plane and the (111) plane, both indicated with (differently) dashed lines. This shift is equivalent to a stacking fault of the (111) planes which are under an angle of 55° with the horizontal (111) planes. Thus, to obtain purely fcc stacked crystals in all directions, interstitials and epitaxial lattice mismatches should be avoided. Large stacking-fault free domains were observed in our crystals as well, demonstrating the feasibility of growing NaCl crystals without stacking defects.

Conclusions and Outlook

We have demonstrated that the crystallization of binary colloidal crystals with a NaCl structure from a binary hard-sphere dispersion can be manipulated by using several external fields (and combinations thereof), i.e., gravity, electric fields, epitaxial templates and dielectrophoretic compression. Initially, with applications in the field of photonics in mind, we aimed at oriented, defect-poor NaCl crystals with large domains and without stacking faults. Combining epitaxial growth on a directing template with dielectrophoretic compression to avoid separation of the dispersion by gravity, we obtained thick, oriented, pure NaCl single crystals with a stoichiometry relatively close to 1. Stress-related stacking faults can appear in the crystal because of the mismatch with the epitaxial template or because of interstitials. The fact that we already demonstrated the growth of hcp crystals grown on a template, together with the small energy difference calculated in this paper between NaCl and NiAs crystals, indicates that the methods used in this paper can also be directly applied to grow NiAs binary crystals. Moreover, although it was not the focus of this paper, the results obtained on homogeneous nucleation induced by the electric-field gradients point out that this methodology is also quite interesting to study the so far experimentally unexplored and fundamentally quite important nucleation of binary crystals.

The obtained results could still be improved on in future experiments by combining the last method with an additional horizontal electric field. By switching off the field afterward and letting the crystal relax to avoid a small lattice distortion in the electric-field direction, further optimization is still possible. However, this combination of all four external fields requires a more advanced electrode arrangement and accurate fine-tuning of experimental procedures to speed up the crystallization on the bottom wall while avoiding homogeneous nucleation in the bulk. Nevertheless, even a NaCl structure with an incomplete filling of smaller spheres could yield interesting optical properties, as was demonstrated by Pursiainen et al. (5).

Materials and Methods

Particle Synthesis and Dispersions. We synthesized two batches of monodisperse core-shell silica spheres. The small spheres, of which the core was labeled with RITC dye, were grown according to the method described by Verhaegh et al. (36) with three modifications to prevent aggregation and secondary nucleation: The time between the addition of tetra ethoxy silane and the addition of dye was adjusted to 8 min, the labeled cores were kept in the Stöber mixture of ammonia and ethanol until a 20-nm unlabeled shell was grown around them, and centrifugation was limited to 50 g. The large spheres, of which the core was labeled with FITC dye, were grown from existing cores by using the Giesche seeded growth (37). The RITC-labeled colloids had a diameter of 412 nm, the polydispersity in size was 5%. The FITC-labeled colloids had a diameter of 1.37 μm, the polydispersity in size was 3.3%. Both particle sizes and polydispersities were determined from static light scattering data.

The silica particles were transferred from the synthesis mixture to the dispersion solvent (DMSO or a glycerol/water mixture) by several centrifugation steps. The glycerol/water mixture was made in a ratio such that it matched the refractive-index of the particles. The initial volume fraction of the DMSO dispersions was 22–24%, the starting colloid volume fraction of the glycerol/water dispersions was 20–22%.

Sample Cell Design. The experiments, in which an external electric field was applied, were performed in sample cells consisting of two glass slides (a #1 cover slide and a microscope slide) with two 50-μm diameter nickel wires in between (spacing between the wires: 1.3 mm) (Fig. 2*A*). The sides of the cell parallel to the wires were closed with candle wax. The other sides were closed with two-component glue (Bison Epoxy Rapide) after filling the cell. The final sample volume was typically 1.3 mm × 2 cm × 50 μm.

Sedimentation experiments on a template were done in a sample cell made of two #1 cover slips, with two #00 glass strips as spacers. On the bottom of the lower cover slide, the square hole array was made by soft lithography (34) in Norland Optical Adhesive 68, which was cured with a UV lamp (wavelength ≈350 nm) for 2 h. The cell was sealed with Norland Optical Adhesive 68. The sample compartment was typically 1 cm × 1 cm × 100 μm.

The compression by dielectrophoresis was done in a sample cell (Fig. 2*B*) with parallel plate electrodes ≈140 μm apart, with a 1-mm slit in both electrodes. The electrodes were made by sputter coating a 10-nm layer of gold on top of a 3-nm layer of chromium (to increase the wetting of the gold) on a cover slide. Two #00 glass strips were used as spacers. Also in this cell, a template was made on the bottom of the lower cover slide by using soft lithography. The sample compartment was similar in size to the sample cells for sedimentation on a template.

Vermolen et al.

Sample Characterization. The 3D structure of all samples was imaged by using a confocal scanning laser microscope (Leica, type NT or SP2). The fluorescent dye FITC was excited with the 488-nm line of an Ar laser, the dye RITC was excited with the 543-nm line of a green HeNe laser. On the SP2 confocal, the signals of these different dyes can be sequentially scanned line by line.

One of the samples, grown by sedimentation on a wall structured by soft lithography with a square template, was dried and imaged by using scanning electron microscopy (Phenom, FEI). The crystal was removed from the substrate and imaged from the bottom side (against the gravity direction) (see Fig. S2).

Image Analysis. The stacking parameter of the structure $\alpha = 1 - (\kappa/P - 2)$ was determined from xz scans of the (110) plane, where κ is the number of twinning planes and P is the number of planes. This gives $\alpha = 1$ for fcc lattices and $\alpha = 0$ for hcp lattices.

We calculated the number ratio $f_N^{crystal}$ in the crystal by determining the coordinates of the particles of several confocal xyz stacks by using IDL software based on methods described by Crocker and Grier (38). The number of small particles (excluding the groups of small particles in vacancies of the crystal of large particles) was divided by the number of large particles to give the number ratio. The number ratios of multiple image stacks were averaged to give $f_N^{crystal}$.

Crystal Stability. The excess Helmholtz free energy, including finite-size correction, of NaCl and NiAs was determined at packing fractions of 0.7 and 0.74 by using the Frenkel and Ladd method (39, 40). The finite-size scaling of the excess free energy was treated as in ref. 40. The corresponding Gibbs free energy was determined as a function of pressure by using thermodynamic integration. We determined the equation of state by using Monte Carlo simulations.

1. Becker K, et al. (2006) Electrical control of förster energy transfer. *Nat Mater* 5:777–781.
2. Shevchenko EV, Talapin DV, Murray CB, O'Brien S (2006) Structural characterization of self-assembled multifunctional binary nanoparticle superlattices. *J Am Chem Soc* 128:3620–3637.
3. Urban JJ, Talapin DV, Shevchenko EV, Kagan CR, Murray CB (2007) Synergism in binary nanocrystal superlattices leads to enhanced p-type conductivity in self-assembled pbte/ag^{-2} te thin films. *Nat Mater* 6:115–121.
4. Redl FX, Cho KS, Murray CB, O'Brien S (2003) Three-dimensional binary superlattices of magnetic nanocrystals and semiconductor quantum dots. *Nature* 423:968–971.
5. Pursiainen OLJ, et al. (2007) Nanoparticle-tuned structural color from polymer opals. *Optics Express* 15:9553–9561.
6. Bartlett P, Pusey PN, Ottewill RH (1991) Colloidal crystallization under time-averaged zero gravity. *Langmuir* 7:213–215.
7. Bartlett P, Ottewill RH (1994) Gravitational effects on the phase-behavior of dispersions. *Adv Colloid Interface Sci* 50:39–50.
8. Christova CG (2005) Binary colloidal crystals. PhD thesis (Utrecht University, Utrecht).
9. Denton AR, Ashcroft NW (1990) Weighted-density-functional theory of nonuniform fluid mixtures: Application to freezing of binary hard-sphere mixtures. *Phys Rev A* 42:7312–7329.
10. Cottin X, Monson PA (1995) Substitutionally ordered solid-solutions of hard-spheres. *J Chem Phys* 102:3354–3360.
11. Trizac E, Eldridge MD, Madden PA (1997) Stability of the ab crystal for asymmetric binary hard sphere mixtures. *Mol Phys* 90:675–678.
12. Eldridge MD, Madden PA, Pusey PN, Bartlett P (1995) Binary hard-sphere mixtures—A comparison between computer-simulation and experiment. *Mol Phys* 84:395–420.
13. Dijkstra M, van Roij R, Evans R (1999) Phase diagram of highly asymmetric binary hard-sphere mixtures. *Phys Rev E* 59:5744–5771.
14. Saunders AE, Korgel BA (2005) Observation of an ab phase in bidisperse nanocrystal superlattices. *Chemphyschem* 6:61–65.
15. Bartlett P, Campbell AI (2005) Three-dimensional binary superlattices of oppositely charged colloids. *Phys Rev Lett* 95:128302.
16. Velikov KP, Christova CG, Dullens RPA, van Blaaderen A (2002) Layer-by-layer growth of binary colloidal crystals. *Science* 296:106–109.
17. Hunt N, Jardine R, Bartlett P (2000) Superlattice formation in mixtures of hard-sphere colloids. *Phys Rev E* 62:900–913.
18. Tommaseo G, et al. (2007) Hypersonic acoustic excitations in binary colloidal crystals: Big versus small hard sphere control. *J Chem Phys* 126:014707.
19. Woodcock LV (1997) Entropy difference between the face-centred cubic and hexagonal close-packed crystal structures. *Nature* 385:141–143.
20. Hoogenboom JP, Derks D, Vergeer P, van Blaaderen A (2002) Stacking faults in colloidal crystals grown by sedimentation. *J Chem Phys* 117:11320–11328.
21. van Blaaderen A, Ruel R, Wiltzius P (1997) Template-directed colloidal crystallization. *Nature* 385:321–324.
22. Dassanayake U, Fraden S, van Blaaderen A (2000) Structure of electrorheological fluids. *J Chem Phys* 112:3851–3858.
23. Hoogenboom JP, van Langen-Suurling AK, Romijn J, van Blaaderen A (2003) Hard-sphere crystals with hcp and non-close-packed structure grown by colloidal epitaxy. *Phys Rev Lett* 90:138301.
24. Yethiraj A, Thijssen JHJ, Wouterse A, van Blaaderen A (2004) Large-area electric-field-induced colloidal single crystals for photonic applications. *Adv Mater* 16:596–600.
25. Yethiraj A, Wouterse A, Groh B, van Blaaderen A (2004) Nature of an electric-field-induced colloidal martensitic transition. *Phys Rev Lett* 92:058301.
26. Hoogenboom JP, van Langen-Suurling AK, Romijn J, van Blaaderen A (2004) Epitaxial growth of a colloidal hard-sphere hcp crystal and the effects of epitaxial mismatch on crystal structure. *Phys Rev E* 69:051602.
27. Leunissen ME, Sullivan MT, Chaikin PM, van Blaaderen A (2008) Dielectrophoretic compression of colloids in an electric bottle. i. Particle transport and growth mechanism of hard-sphere-like crystals. *J Chem Phys* 128:164508.
28. Hollingsworth AD, Saville DA (2004) Dielectric spectroscopy and electrophoretic mobility measurements interpreted with the standard electrokinetic model. *J Colloid Interface Sci* 272:235–245.
29. Hynninen AP, Dijkstra M (2005) Phase diagram of dipolar hard and soft spheres: Manipulation of colloidal crystal structures by an external field. *Phys Rev Lett* 94:138303.
30. Royall CP, Dzubiella J, Schmidt M, van Blaaderen A (2007) Nonequilibrium sedimentation of colloids on the particle scale. *Phys Rev Lett* 98:188304.
31. Wysocki A, et al. (2009) Direct observation of hydrodynamic instabilities in a driven non-uniform colloidal dispersion. *Soft Matter* 5:1340–1344.
32. Thijssen JHJ, et al. (2006) Characterization of photonic colloidal single crystals by microradian X-ray diffraction. *Adv Mater* 18:1662–1666.
33. Sullivan MT, et al. (2006) An electric bottle for colloids. *Phys Rev Lett* 96:015703.
34. Hoogenboom JP (2002) Colloidal epitaxy: A real-space analysis. PhD thesis (Utrecht University, Utrecht).
35. Vermolen ECM (2008) Manipulation of colloidal crystallization. PhD thesis (Utrecht University, Utrecht).
36. Verhaegh NAM, van Blaaderen A (1994) Dispersions of rhodamine-labeled silica spheres—Synthesis, characterization, and fluorescence confocal scanning laser microscopy. *Langmuir* 10:1427–1438.
37. Giesche H (1994) Synthesis of monodispersed silica powders. 1. Particle properties and reaction-kinetics. *J Eur Ceram Soc* 14:189–204.
38. Crocker JC, Grier DG (1996) Methods of digital video microscopy for colloidal studies. *J Colloid Interface Sci* 179:298–310.
39. Frenkel D, Ladd AJC (1984) New monte carlo method to compute the free energy of arbitrary solids. application to the fcc and hcp phases of hard spheres. *J Chem Phys* 81:3188–3193.
40. Polson JM, Trizac E, Pronk S, Frenkel D (2000) Finite-size corrections to the free energies of crystalline solids. *J Chem Phys* 112:5339–5342.

APPLIED PHYSICAL SCIENCES